Journal of Aerosol Science 151 (2021) 105661

Contents lists available at ScienceDirect

Journal of Aerosol Science

journal homepage: http://www.elsevier.com/locate/jaerosci

Risk assessment of airborne transmission of COVID-19 by asymptomatic individuals under different practical settings

Siyao Shao [a,b], Dezhi Zhou [a], Ruichen He [a,b], Jiaqi Li [a,b], Shufan Zou [a], Kevin Mallery [a,b], Santosh Kumar [a,b], Suo Yang [a,**], Jiarong Hong [a,b,*]

[a] Department of Mechanical Engineering, 111 Church ST SE, University of Minnesota, Minneapolis, MN, 55414, USA
[b] Saint Anthony Falls Laboratory, 2 3rd AVE SE, University of Minnesota, Minneapolis, MN, 55414, USA

ARTICLE INFO

Keywords:
Airborne transmission
Exhaled particles
Digital inline holography
Particle contamination
Ventilation

ABSTRACT

The lack of quantitative risk assessment of airborne transmission of COVID-19 under practical settings leads to large uncertainties and inconsistencies in our preventive measures. Combining *in situ* measurements and computational fluid dynamics simulations, we quantify the exhaled particles from normal respiratory behaviors and their transport under elevator, small classroom, and supermarket settings to evaluate the risk of inhaling potentially virus-containing particles. Our results show that the design of ventilation is critical for reducing the risk of particle encounters. Inappropriate design can significantly limit the efficiency of particle removal, create local hot spots with orders of magnitude higher risks, and enhance particle deposition causing surface contamination. Additionally, our measurements reveal the presence of a substantial fraction of faceted particles from normal breathing and its strong correlation with breathing depth.

1. Introduction

The global pandemic of COVID-19 (caused by the SARS-CoV-2) has demonstrated the extraordinary transmissibility of the virus, with more than 11 million people infected as of writing. However, mechanisms to contain the disease are regionally variable, with vastly different approaches being utilized by different countries, regions (such as US states), and even cities (Anderson et al., 2020). This inconsistency is due in part to a lack of understanding of the transmission pathways of the disease (Anderson et al., 2020). Although it has been well-accepted that the disease can be transmitted through large droplets (>5 μm) capable of carrying sufficient viral load produced by coughing and sneezing (Gralton et al., 2011; World Health Organization, 2004), there is substantial debate regarding whether the transmission can be airborne with small droplets (Asadi et al., 2020; Lewis, 2020; Prather et al., 2020). Nevertheless, growing evidence, including the detection of SARS-CoV-2 RNA in collected particles (Liu et al., 2020) and the ability of SARS-CoV-2 to remain viable for hours in particles (van Doremalen et al., 2020), indicates such a transmission pathway is possible. Moreover, considering the high viral loads found in the upper respiratory tract of asymptomatic individuals infected with COVID-19 (Zou et al., 2020), it has been hypothesized that small droplets and particles generated during normal respiratory behaviors, such as breathing and speaking, could lead to the fast spread of the disease (Edwards et al., 2004; Fabian et al., 2008, and Johnson and Morawska, 2009). However, despite a number of studies of particle generation from these behaviors (Chao et al., 2009; Haslbeck et al.,

* Corresponding author. Department of Mechanical Engineering, 111 Church ST SE, University of Minnesota, Minneapolis, MN, 55414, USA.
** Corresponding author.
E-mail addresses: suo-yang@umn.edu (S. Yang), jhong@umn.edu (J. Hong).

https://doi.org/10.1016/j.jaerosci.2020.105661
Received 24 July 2020; Received in revised form 31 August 2020; Accepted 3 September 2020
Available online 16 September 2020

2010; Heo et al., 2017; Johnson and Morawska, 2009; Papineni & Rosenthal, 1997), there is a lack of *in situ* characterization (i.e., with minimal interference on human respiratory behaviors and without potentially lossy sample collecting procedures), limiting our ability to model the spread of particles associated with asymptomatic individuals. This is particularly true for breathing due to its low particle production rate. Specifically, most studies on the size distribution of such particles use devices such as aerodynamic particle sizers (APS) and optical particle counters (OPC) which require transporting the particles to the sensor and do not account for particle evaporation and particle losses during the transport (Bake et al., 2019). The only *in situ* measurement (Chao et al., 2009) utilizes interferometric Mie imaging (IMI), which captures particles above 2 μm with measurement accuracy depending on the assumptions of particle refractive index and shape (assumed to be spherical). It is worth noting that recent *in situ* measurements of speech-generated particles using laser sheet imaging with an iPhone 11 camera (Stadnytskyi et al., 2020) was carried out with high speaking volume (>59 dB) which should not be considered as normal respiratory behaviors. Accordingly, no study has conducted computational fluid dynamics (CFD) simulation of the change of size and concentration of particles over time and their spatial variation in an enclosed environment to provide quantitative assessment of the risk of airborne infection. These models are necessary for producing scientifically driven policy regarding social distancing measures and safe business re-opening.

Therefore, in the current study, we present the first detailed characterization of the particle generation process of normal human breathing by combining quantitative Schlieren imaging and multi-magnification digital inline holography (DIH). Such measurements, conducted with eight participants, provide the instantaneous and ensemble average flow field of exhaled gas as well as the concentration, size, and shape distributions of particles ranging from 0.5 to 50 μm within it. This information is then used as the inputs for high-fidelity CFD simulation of particle transport under several practical settings, which considers the evaporation, drag, gravity, and residence lifetime of each particle produced by a simulated asymptomatic individual. The simulation results are then used to assess the potential of airborne disease transmission associated with the normal respiratory behaviors under these settings.

2. Methodology

In the breathing experiment, a participant is seated and instructed to breath using a nose inhale and mouth exhale at a rate of 15.2 breaths per minute with a 2:3 inhalation-exhalation ratio, within the range of normal breathing patterns (Tobin et al., 1983). During the experiments, a mouthpiece is used to align the breathing direction with the measurement volume of the high-speed Schlieren and holographic measurements (see Fig. S1 in the supplementary materials). The participate first breathes five times in front of a high-speed Schlieren imaging setup (Fig. S3 in the supplementary materials). The acquired Schlieren images are then processed using optical flow method to determine the instantaneous and averaged flow fields of normal breathing (Liu & Shen, 2008), from which the instantaneous/averaged volumetric flow rate and spatial extent of the exhaled flow are obtained (Table S1 in the supplementary materials). Subsequently, digital inline holography (DIH) measurements are conducted to determine the particle generation from breathing. DIH is an optical diagnostic technique which allows *in situ* imaging of individual microparticles in an extended sample volume (i.e., orders of magnitude larger than conventional microscopy in the imaging depth of field) without focusing (Poon & Liu, 2014; Katz & Sheng, 2010, and Yu et al., 2014). In our experiment, DIH measurements with both 1X (with a pixel resolution of 4.5 μm/pixel, Figs. S5 and S6 in the supplementary materials) and 20X (with a pixel resolution of 0.23 μm/pixel, Figs. S8 and S9 in the supplementary materials) magnifications are implemented to capture the particles from above and below 5 μm, respectively. The sample volumes of DIH with both magnifications are positioned 1.5 cm away from the mouth to capture *in situ* the original forms of particles generated directly from breathing with minimal influence of evaporation. For DIH measurement with each magnification, the participant is instructed to breath in the same fashion seating in front of the DIH setup for 20 min (30 s breathing alternates with 30 s rest, in total 10-min breathing data). The DIH data (i.e., holograms) with exhaled particles present in the sample volume are first selected, and subsequently reconstructed using Rayleigh-Sommerfeld diffraction kernel (Katz and Sheng 2010). The reconstructed holograms are then processed using automatic image analysis software validated with manual checking using ImageJ to determine the concentration, size (in terms of equivalent diameter), and shape (in terms of circularity, Fig. S8 in the supplementary materials) of particles generated from breathing. The breathing experiment described above is conducted over in total eight participants with varying gender and age. The data from all the participants are compiled to obtain the ensemble-averaged results used as the inputs for the CFD simulations. The size range of particles during simulation is set to be from 0.5 to 50 μm following the size distribution of particles exhaled during breathing measured from experiments. It is worth noting that the small particles (<5 μm) are primarily responsible for airborne transmission due to their long residence time according to Asadi et al. (2020), Lewis (2020), and Prather et al. (2020). The simulation is used to model the distribution and accumulation of particles under different practical settings. The CFD simulations are conducted using the OpenFoam-6 platform, with the Eulerian-Lagrangian framework for the gas liquid phase simulation (Jasak et al., 2007). Three practical settings (i.e., elevator, small classroom, and small supermarket) are chosen for the simulation. For each setting, different ventilation conditions are simulated to study the effects of ventilation on the dispersion of the exhalation particles. During the simulation, the room ventilation rate is set to be 30 air changes per hour (ACH) except for the low ventilation elevator case (2 ACH). It is worth noting that ACH is a commonly used unit in the room ventilation community, especially for studies of airborne disease transmission (Mangili & Gendreau, 2005; Memarzadeh & Xu, 2012). Considering the room temperature and 40% humidity in this study, the classical evaporation model based on quasi-steady-state assumption is used to account for the evaporation of droplets (Ranz & Marshall, 1952). Based on our experimental observation, we also assume all the large droplets will eventually evaporate into residual particles of 1.5 μm, i.e., a threshold corresponding to the peak of our particle size distribution measured in our breathing experiments (representing the most-probable residue size). The detailed reasoning of this assumption is provided in the Results Section and supplementary materials. All the injected particles are tracked by the simulation model described in the supplementary materials. The simulation model stops tracking the particles once they encounter surfaces such as walls and

considers the particles deposited on the surfaces. The details of experiment and CFD simulation are provided in the supplementary materials.

3. Results

3.1. In situ measurements of particle generation during normal breathing

The ensemble average flow field of exhaled gas (Fig. 1A), characterized using quantitative Schlieren imaging, shows an axisymmetric cone shape with an averaged cone angle ($\overline{\theta}$) of 25.0°. The streamwise flow velocity averaged over the cross section of the exhalation cone ($\overline{u}$) decays from 0.3 m/s near the mouth to almost zero at about 200 mm (<1 feet) downstream. These measurements demonstrate the limited spatial range of direct influence associated with normal breathing, in contrast to violent expiratory behaviors such as coughing which yields a cone angle of 65° (Gupta et al., 2009) and flow speed up to 11.2 m/s with the influence zone extending up to ~2.5 m (Bourouiba et al., 2014). The exhaled gas flow fields from different participants show similar patterns with small variation in quantitative measures (e.g. cone angle, exhaled flow rate, exhaled flow velocity etc., Table S1 with details in the supplementary materials). The normalized exhaled gas flow rate ($\widehat{Q}_E$) in an exhalation cycle (period T_E) extracted from flow field, rises sharply at the beginning of the cycle, peaks around 0.2 T_E followed by a sustained rate over a duration of about 0.3 T_E, and then decays rapidly (Fig. 1B). Such breathing pattern is similar across different participants as they are instructed to breath in the same fashion, but the peak value of $\widehat{Q}_E$ ($\widehat{Q}_{E,max}$) varies substantially among individuals (Fig. S4 in the supplementary materials) potentially due to different natural breathing depths of each individual (Miserocchi and Milic-Emili, 1976; Ganong, 1995, and Benchetrit, 2000).

The DIH measurements provide the first detailed characterization of the generation of particles during normal breathing in terms of their concentration, size, and shape. The measurements have shown an average concentration of 170 particles per liter exhaled gas (i.e., 44 particles per breath) from an ensemble average of 160 min DIH data from eight participants. The particle size distribution peaks around 1.5 μm with a sharp decay towards smaller and larger sizes and has an averaged value of 1.7 μm (Fig. 1C), which is substantially higher than the 0.6 μm obtained from OPC measurement (Papineni et al., 1997) and close to the 2 μm measured using microscopic examination of particles deposited on a glass slide through an impactor (Papineni et al., 1997). Most particles are below 5 μm and only

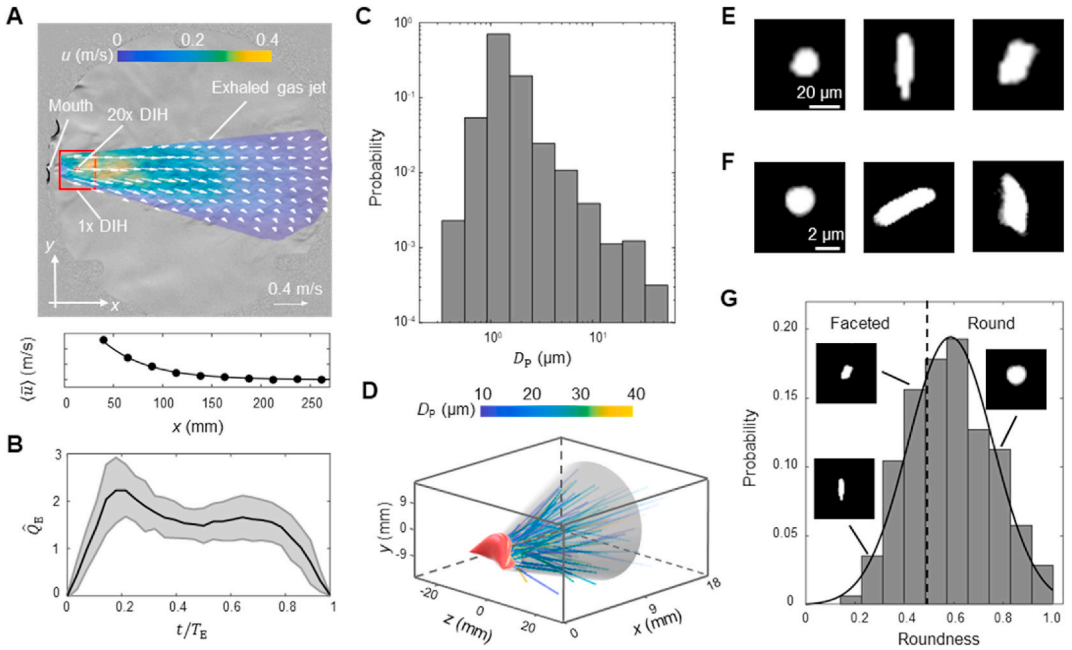

Fig. 1. (**A**) The ensemble average flow field of exhaled gas of all participants superimposed onto an enhanced Schlieren image sample of exhaled gas flow. The details of generating this figure can be found in the supplementary materials. The locations of the mouth, the sampling windows of 1X and 20X digital inline holography (DIH) are marked in the figure. Additionally, the streamwise velocity averaged over the cross section of the exhalation cone ($\overline{u}$) is plotted against the streamwise distance to the mouth (x) to show the decay of flow velocity. (**B**) The change of the normalized exhaled gas flow rate ($\widehat{Q}_E$) in one exhalation cycle of time period T_E, where $\widehat{Q}_E$ is the instantaneous exhaled gas flow rate (Q_E) divided by its average for each exhalation cycle. The solid curve and shaded area represent the ensemble average and variance of $\widehat{Q}_E$ of all participants, respectively. (**C**) The histogram of particle size quantified using area equivalent diameter (D_P). (**D**) The 3D trajectories of all the particles captured using 1X magnification DIH. Sample images of particles from (**E**) 1X and (**F**) 20X DIH measurements. (**G**) The histogram of particle shape quantified using particle roundness (Fig. S7 with details in the supplementary materials) with inset figures showing samples of particles with different roundness levels. The solid line is the fitted normal distribution and the dashed line corresponds to the roundness of 0.5.

0.2% above. The 3D trajectories of particles (>5 μm) within the exhaled gas fit within the breathing cone determined from the Schlieren imaging for all the participants with about 10% particles leaking from the side of the mouth occasionally (Fig. 1D). Besides the particle size, the shape of particles can be obtained using DIH. Interestingly, in addition to a large fraction of round-shaped particles, a substantial fraction yields irregular shapes with edges and corners. Observed both above (Fig. 1E) and below 5 μm (Fig. 1F), these two types of particles with distinct shapes correspond respectively to the droplets and faceted particles generated from human breathing reported in the literature (Papineni et al., 1997, Morozov and Mikheev 2017). Particularly, through mass spectra of particles, the literature has revealed the presence of nonvolatile solutes such as potassium, calcium, and chorine contents in the faceted particles (Papineni et al., 1997, and Morozov & Mikheev, 2017), which are likely to be generated from the alveolar fluid from the lower respiratory tract (Johnson & Morawska, 2009). In addition, Morozov and Mikheev (2017) suggested that these faceted particles can contain lipids and hydrophobic proteins which are soluble in organic solvents. Noteworthily, such faceted particles could be the residues of droplet evaporation and may correspond to the long-lasting dry particles reported in the experiments of Stadnytskyi et al. (2020). This information serves as the basis for setting the residue size for droplet evaporation in our simulation (detailed reasoning provided in the supplementary materials). To quantify the content of particles based on their shapes, the histogram of roundness of particles (Fig. S7 with details in the supplemental materials), is obtained (Fig. 1G), and a roundness threshold of 0.5 is selected to categorize the particles into droplet and faceted types according to the literature (Powers, 1953, and Hamilton & Adie, 1982). Accordingly, our measurements suggest about 33% of particles produced by normal breathing are faceted type appearing both below and above 5 μm (Fig. S12 shows that particle roundness is independent with the size). These faceted particles are usually hygroscopic (Morozov and Mikheev 2017) and could take up moisture from the environment with increasing humidity to form droplets up to 2.5 times of their original sizes (Zieger et al., 2017). It has been suggested moisture can insulate viruses from extreme environments, in favor of their survival during transmission (Tang, 2009). Therefore, these faceted particles may serve as the major virus carriers for airborne transmission since they are likely to the final products of droplet evaporation and can last substantially longer in the air.

3.2. *Variation of particle generation across different participants*

The particle measurements exhibit interesting variability across different participants using the same normal breathing techniques

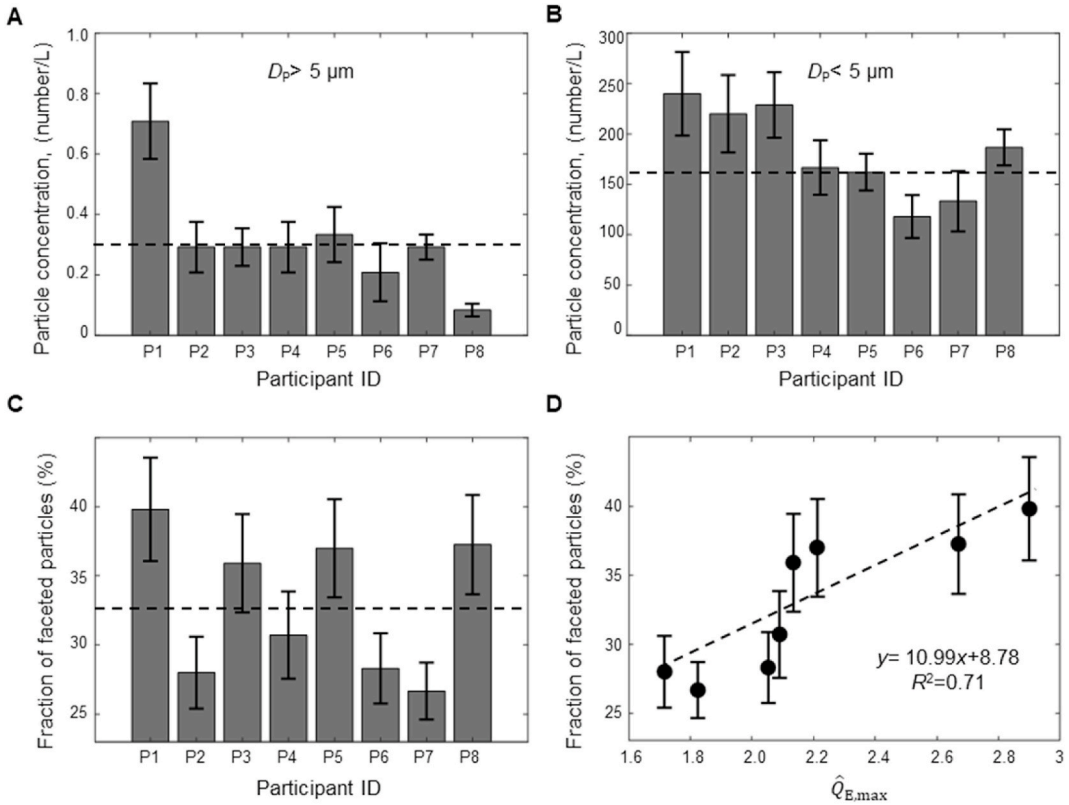

Fig. 2. The variation of particle concentration (number/L) across different participants for (**A**) particles larger than 5 μm and (**B**) smaller than 5 μm. The dashed lines in the figures correspond to the average particle concentration. (**C**) The variation of the fraction of faceted particles across different participants with its average value marked by the dashed line in figure. (**D**) The variation of the fraction of faceted particles with respect to the normalized peak exhaled gas flow rate ($\widehat{Q}_{E,max}$) of each participant. The dashed line and the equation in the figure are the least square linear fit of the data.

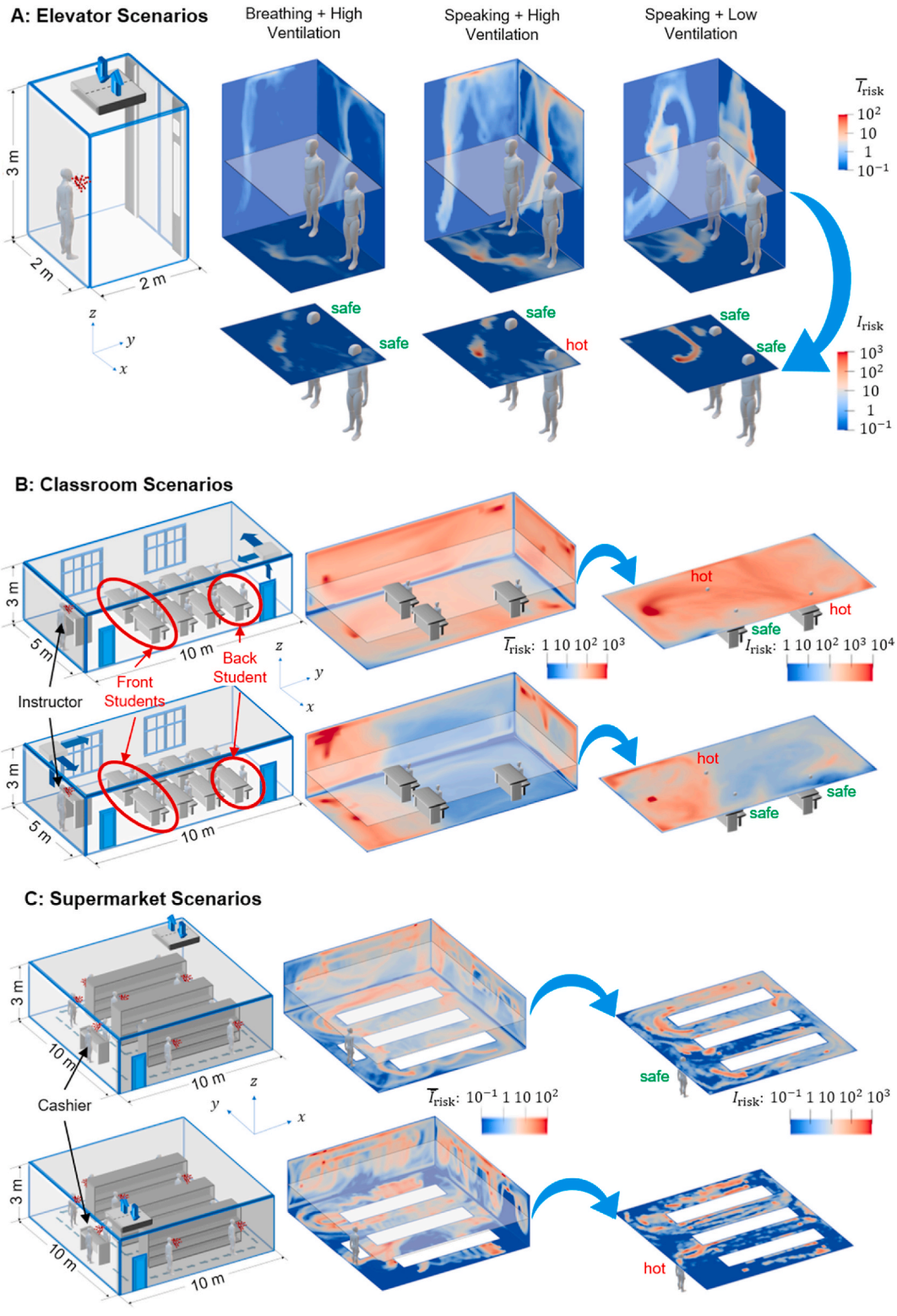

(caption on next page)

Fig. 3. The CFD simulation of particle transport and deposition to evaluate the risk under (**A**) an elevator setting with a simulated asymptomatic individual breathing under high ventilation of 30 ACH (supplementary movie S1), speaking under high ventilation (supplementary movie S2) and low ventilation of 2 ACH (supplementary movie S3), (**B**) a small classroom setting with a simulated asymptomatic instructor and the ceiling ventilation system located in the back (the top part of the figure, supplementary movie S4) and front of the classroom (the bottom part of the figure, supplementary movie S5), respectively, and (**C**) a small supermarket setting with a simulated asymptomatic shopper (his/her 10 stops along the dashed route are marked in the schematic) and the ceiling ventilation system located at the back corner (the top part of the figure, supplementary movie S6) and entrance of the supermarket (the bottom part of the figure, supplementary movie S7), respectively. Except for the low ventilation setting in **A**, the ventilation rate of each setting is designed to replace all the air in the space every 2 min, representing the upper bound of recommended ventilation condition of each setting. Under each setting, the risk of a person encountering virus-containing particles at one specific location (I_{risk}) is evaluated as the total particle number passing through this location during the simulation time, which can be interpreted as number of particles a person can inhale at this location during the simulated time. Note that such an estimate of the inhaled particle number only provides an estimate of maximum particle encounter since it does not consider the detailed flow processes involved in the inhalation of particles. In the 3D contour plots, the wall contours are the contours of I_{risk} spatially averaged (denoted as $\bar{I}_{risk}$) along x, y, and z directions, respectively. In addition, assuming the height of each individual is ~1.75 m, selected horizontal slices of I_{risk} contour at the height of human mouth are highlighted to show the I_{risk} for individuals standing (1.6 m for **A** and **C**) or sitting (1.2 m for **B**) at different locations, and several representative locations are marked as safe or hot based on their I_{risk} values (safe criterion: $I_{risk} \leq 1$ for **A**; $I_{risk} \leq 200$ for **B**; $I_{risk} \leq 100$ for **C**; note that safe or hot zones are determined based on the overall I_{risk} in each setting).

(Fig. 2). Specifically, the concentration of particles larger than 5 μm varies significantly across different individuals (Fig. 2A) while the particles smaller than 5 μm do not show such large variation (Fig. 2B). In particular, the concentration of particles larger than 5 μm produced by one participant (P1) is more than twice the average concentration of the eight participants. Considering particles in this scale range contain higher viral loads (Alonso et al., 2015, and Zhai et al., 2018) and can evaporate rapidly to be airborne, such an individual can be more effective in spreading viruses when asymptomatic. It is worth noting that other studies on particle generation during breathing and speaking also reported the presence of such superemitters, with population percentage ranging from 6% to 25% (Johnson & Morawska, 2009; Asadi et al., 2019), consistent with the percentage of such individual (12.5%) observed in our experiments. Superemitters of particles have been related to the superspreaders of infectious diseases in the literature (Edwards et al., 2004; Asadi et al., 2019; Hamner, 2020). Remarkably, the percentage of superemitters in our study (though there is large uncertainty due to the small sample size) coincides well with the 10% of superspreading events of COVID-19 observed in preliminary clinical data (Endo et al., 2020), providing further support to the spreading of COVID-19 through particle generation from asymptomatic individuals. In addition, the fraction of faceted particles varies from 26% to 40% across different participants (Fig. 2C), and correlates with the peak of normalized exhaled flow rate ($\widehat{Q}_{E,max}$) defined earlier (Fig. 2D). Considering the connection between $\widehat{Q}_{E,max}$ and the natural breathing depth of individuals as noted earlier (Benchetrit, 2000; Ganong, 1995; Miserocchi & Milic-Emili, 1976), our results indicates that the deeper exhalation can lead to the generation of a higher fraction of faceted particles from the lower respiratory tract as suggested in the literature (Johnson & Morawska, 2009).

3.3. *The CFD simulation of particle transport and deposition under different practical settings*

Using the flow and particle information derived from our breathing experiments, CFD simulations are conducted under three practical settings to determine the particle transport and deposition and assess the risk of being infected (I_{risk}) through the airborne transmission of COVID-19 caused by asymptomatic individuals (details of simulation in materials and methods in supplementary materials).

Under the elevator setting (Fig. 3A), a simulated asymptomatic individual (referred to as the “emitter” hereafter) is placed near the wall opposite to the door for 1 min. With high ventilation, the particles from the emitter disperse to a large portion of the elevator within 1 min, but I_{risk} is extremely low ($\leq$1) in most of the space (e.g., the two “safe” spots). To assess a riskier scenario, we consider the emitter speaking continuously for 1 min and producing particles at a rate 10 times that of normal breathing according to the literature (Asadi et al., 2019). Without changing ventilation, this scenario exhibits a proportional increase in I_{risk} and the expansion of regions with high risks (e.g., the “hot” spot). With significant reduction in ventilation, the dispersion of particles is confined to one quadrant of the elevator on the emitter side, imposing little risk to the people who are not standing in close proximity to the emitter (e.g., in the two “safe” spots) but two orders of magnitude higher risks for some local hot spots in the quadrant. Remarkably, even under high ventilation, only a small fraction (~15%) of particles is vented out, and the number drops to zero with reduced ventilation. This observation is associated with the presence of stable flow circulation zones in the space (Fig. S15, which traps the particles and increases their residence time to be significantly longer than the simulated time here. In addition, such circulation zone strengthens with increasing ventilation causing more wall deposition of particles (Fig. S16).

Under the small classroom setting (Fig. 3B), we consider the emitter to be the instructor upfront and the particles are continuously produced through speaking for 50 min (the typical duration of a lecture), representing a much riskier scenario in comparison to one of the breathing students being the emitter. When the ceiling ventilation is at the back corner in the classroom (i.e., far from the emitter), the ventilation spreads particles to the back half of the classroom. Particularly, the region near the vent can yield a significantly higher I_{risk}, such that a student sitting in a hot spot in the back could inhale several times more particles than a front student at a safe spot. As the ventilation is relocated to the emitter side, the spread of particles is mostly confined to the region before the front students and the I_{risk} for each student is significantly reduced compared to the former scenario. Remarkably, despite the rate of ventilation set to replace all the air in the space every 2 min for both scenarios, no more than 10% of the total emitted particles are vented out after 50 min,

although the latter (i.e., ventilation near the emitter) doubles the fraction of vented-out particles of the former (Table S2). Such inefficient particles removal through ventilation is largely associated with the presence of many stable circulation regions in the large space (Fig. S19), which increases particle residence time, causes the majority of particles deposited to surfaces (i.e., 88% of the total, Table S2), and forms hot spots of surface contamination (e.g., the two ground corners on the same side of the classroom for both ventilation scenarios, Fig. S18).

Under a small supermarket setting (Fig. 3C), the emitter is considered as an asymptomatic shopper with regular breathing, who makes 10 stops (3 min for each stop with the last stop at the cashier) along a designated zigzag shopping path for 30 min. When the ceiling ventilation is in the back corner, the particles spread across the entire supermarket, and particularly, a hot spot is formed in the space between the leftmost shelf and corner near the ventilation due to strong local circulation and entrainment of higher speed channeling flow formed in this space (Fig. S17). However, the cashier, standing near the entrance, is placed in a relatively safe zone. With the ventilation moved to the entrance, the overall spread of particles is reduced, but several other hot spots emerge, including one in front of the cashier increasing his/her risk by about two orders of magnitude. Compared with the classroom setting, the fraction of vented-out particles (~50% for both scenarios, Table S2) is significantly increased here, even at similar ventilation and shorter time duration. Such increase in the particle removal efficiency is primarily attributed to the motion of the emitter which limits the chance of a large fraction of particles becoming trapped in the same stable circulations. Additionally, due to the presence of dividing structures (i.e., shelves), the stable circulation zones reduce in scale (Fig. S17) in comparison to those under the classroom setting, causing less wall deposition except in the back corner near the ventilation (Fig. S20).

4. Summary and discussions

Combining novel *in situ* measurements and CFD simulations, our study provides a systematic assessment of risks due to airborne transmission of viruses generated by asymptomatic individuals in a confined space under ventilation. Through integrated quantitative Schlieren imaging and digital inline holography (DIH), our experimental measurements provide a detailed *in situ* characterization of particle generation through normal breathing, including natural breathing flow field, size distribution, concentration, and shapes of particles over a broad range of sizes. The normalized exhaled gas flow rate calculated from breathing flow field measured by Schlieren imaging shows similar pattern across different individuals, despite variation of peak exhaled flow rate, due to different natural breathing depth. Our DIH measurements show that most exhaled particles are below 5 μm with only 0.2% above. The measurements further reveal the presence of two types of particles in the exhaled gas, i.e., round and faceted types, based on particle shapes. The concentration of particles shows large variability across different individuals, with the presence of one potential "superemitter" out of eight participants. Such ratio (12.5%) coincides approximately with the 10% of superspreading events of COVID-19 (Endo et al., 2020), providing further support of transmission of COVID-19 through particles generated by asymptomatic individuals. Our measurements have also indicated that the fraction of faceted particles of different participants is strongly correlated with the natural breathing depth of the individual. Our simulation results show significant spatial heterogeneity of risks in confined spaces under three practical settings, supporting the interesting observations of COVID-19 infection associated with air conditioning in a restaurant (Lu et al., 2020). Specifically, although ventilation enables the removal of virus-containing particles, it can help spread particles to larger spaces beyond the proximity of asymptomatic individuals. Inappropriate ventilation can also lead to local hot spots with risks that are orders of magnitude higher than other places depending on the relative positioning of particle emitter, ventilation, and space settings. In addition, ventilation can also enhance particle deposition on surfaces causing patched regions with high surface contamination, consistent with the large amount SARS-CoV-2 RNAs extracted from samples collected from hospital floors and air vents (Liu et al., 2020; Ong et al., 2020). It is also worth noting that these deposited particles (both faceted particles and droplets) can form highly-resilient microscale residues on surfaces, which may shield the viruses from the influence of environmental changes and contribute to the long-lasting surface infectivity reported in van Doremalen et al. (2020) as suggested in a recent study (Kumar et al., 2020). Particularly, ventilation at a single location, even at the highest rate in the current practice, is highly inefficient at removing particles, due to the presence of relatively stable flow circulation zones in the space and the large amount of particle deposition on surfaces. This result suggests that improvements to air filters alone are not enough to reduce the particle concentration.

Our study can directly lead to practical guidelines and science-driven policy for mitigating the risks of airborne infection of COVID-19 with minimal impact on the economy and social activities, which are critical for the safe re-opening of many businesses. Specifically, our results suggest that optimizing ventilation settings (e.g., adding more sites of ventilation) even under the current ventilation capacity can significantly improve the efficiency of particle removal. Adjusting the placement of occupants (e.g., students or cashier in our cases) in the room to avoid hot spots and frequent cleaning of surfaces prone to contamination can reduce the risks. Wearing masks to cut down the source of particle generation can significantly lower the risks of airborne infection. Additionally, our *in situ* characterization of particle generation through breathing shows its large variability and correlation with individual breathing depth, indicating the need for effective risk assessment at an individual level. Our study can be further extended to a broad range of practical settings (e.g., air cabin, restaurant, gym, etc.) with more detailed physics (e.g., exhalation, inhalation flow physics, etc.) and individual characteristics (e.g., exhalation behavior, movement, etc.) as well as more precise HVAC models incorporated to yield more accurate risk assessment under these settings.

Finally, we would like to point out future avenues of research that can be explored according to the findings from the present results. First, by expanding the sample size, the large uncertainty of the findings including the correlation between the superspreading events of COVID-19 and the expired particle size distribution of different individuals as well as the trend of the faceted particle fraction versus natural breathing depth will be adequately addressed. Second, detailed analysis of the influence of optimizing ventilation sites (i.e., adding more ventilation sites) in future simulation studies can provide science-based guidelines for mitigating the risks of COVID-

19 airborne transmission. Third, a validated dose-response model (which is not yet available for COVID-19) should be used to develop an accurate assessment of the probability of airborn infection based on the I_{risk} value presented here (Wan et al., 2009, Morawska et al., 2013). In this paper, the I_{risk} metric used to assess the risk of airborne transmission of COVID-19 is the measure of the number of exhaled particles a person is exposed to at specific location during the simulation time. In other words, this number is the upper limit of the virus-laden particles can be inhaled or contacted by a person during the simulation time. As suggested by Wan et al. (2009) and Moraswska et al. (2013), I_{risk} is directly related to the risk of being infected by diseases through airborne transmission. In addition, the spatial distribution of I_{risk} generated from our simulation can be used to assess the high and low risk zones of the exposure to the virus-laden particles under different practical settings and ventilation conditions.

Funding

Jiarong Hong's group: University of Minnesota Rapid Response Grant from Office for Vice President of Research (OVPR); Suo Yang's group: University of Minnesota Institute for Engineering in Medicine (IEM) COVID-19 Rapid Response Grant program, Co-Sponsored by the Minnesota Robotics Institute (MnRI) and the Clinical and Translational Science Institute (CTSI) through the National Center for Advancing Translational Sciences (NCATS) of the National Institutes of Health (NIH) Award Number UL1TR002494. The content is solely the responsibility of the authors and does not necessarily represent the official views of the National Institutes of Health (NIH).

Data and materials availability

All data is available in the main text or the supplementary materials. All data, code, and materials are hosted at the Data Repository for the University of Minnesota.

Declaration of competing interest

The authors declare that they have no known competing financial interests or personal relationships that could have appeared to influence the work reported in this paper.

Acknowledgments

We thank Hongyuan Zhang for helping out with some visualizations of the numerical data.

Appendix A. Supplementary data

Supplementary data to this article can be found online at https://doi.org/10.1016/j.jaerosci.2020.105661.

References

Alonso, C., Raynor, P. C., Davies, P. R., & Torremorell, M. (2015). Concentration, size distribution, and infectivity of airborne particles carrying swine viruses. *PloS One, 10*(8), Article e0135675.

Anderson, R. M., Heesterbeek, H., Klinkenberg, D., & Hollingsworth, T. D. (2020). How will country-based mitigation measures influence the course of the COVID-19 epidemic? *The Lancet, 395*(10228), 931–934.

Asadi, S., Bouvier, N., Wexler, A. S., & Ristenpart, W. D. (2020). The coronavirus pandemic and aerosols: Does COVID-19 transmit via expiratory particles? *Aerosol Science and Technology, 54*, 1–4.

Asadi, S., Wexler, A. S., Cappa, C. D., Barreda, S., Bouvier, N. M., & Ristenpart, W. D. (2019). Aerosol emission and superemission during human speech increase with voice loudness. *Scientific Reports, 9*(1), 1–10.

Bake, B., Larsson, P., Ljungkvist, G., Ljungström, E., & Olin, A. C. (2019). Exhaled particles and small airways. *Respiratory Research, 20*(1), 8–21.

Benchetrit, G. (2000). Breathing pattern in humans: Diversity and individuality. *Respiration Physiology, 122*(2–3), 123–129.

Bourouiba, L., Dehandschoewercker, E., & Bush, J. W. (2014). Violent expiratory events: On coughing and sneezing. *Journal of Fluid Mechanics, 745*, 537–563.

Chao, C. Y. H., Wan, M. P., Morawska, L., Johnson, G. R., Ristovski, Z. D., Hargreaves, M., & Katoshevski, D. (2009). Characterization of expiration air jets and droplet size distributions immediately at the mouth opening. *Journal of Aerosol Science, 40*(2), 122–133.

Edwards, D. A., Man, J. C., Brand, P., Katstra, J. P., Sommerer, K., Stone, H. A., … Scheuch, G. (2004). Inhaling to mitigate exhaled bioaerosols. *Proceedings of the National Academy of Sciences, 101*(50), 17383–17388.

Endo, A., Abbott, S., Kucharski, A. J., & Funk, S. (2020). Estimating the overdispersion in COVID-19 transmission using outbreak sizes outside China. *Wellcome Open Research, 5*(67), 67.

Fabian, P., McDevitt, J. J., DeHaan, W. H., Fung, R. O., Cowling, B. J., Chan, K. H., … Milton, D. K. (2008). Influenza virus in human exhaled breath: An observational study. *PloS One, 3*(7), Article e2691.

Ganong, W. F. (1995). *Review of medical physiology*. Mcgraw-hill.

Gralton, J., Tovey, E., McLaws, M. L., & Rawlinson, W. D. (2011). The role of particle size in aerosolised pathogen transmission: A review. *Journal of Infection, 62*(1), 1–13.

Gupta, J. K., Lin, C. H., & Chen, Q. (2009). Flow dynamics and characterization of a cough. *Indoor Air, 19*(6), 517–525.

Hamilton, R., & Adie, G. (1982). Size, shape and elemental associations in an urban aerosol. *The Science of the Total Environment, 23*, 393–402.

Hamner, L. (2020). *High SARS-CoV-2 attack rate following exposure at a choir practice—skagit County, Washington, March 2020. MMWR* (Vol. 69). Morbidity and Mortality Weekly Report.

Haslbeck, K., Schwarz, K., Hohlfeld, J. M., Seume, J. R., & Koch, W. (2010). Submicron droplet formation in the human lung. *Journal of Aerosol Science, 41*(5), 429–438.
Heo, K. J., Lim, C. E., Kim, H. B., & Lee, B. U. (2017). Effects of human activities on concentrations of culturable bioaerosols in indoor air environments. *Journal of Aerosol Science, 104*, 58–65.
Jasak, H., Jemcov, A., & Tukovic, Z. (2007). *International Workshop on Coupled Methods in Numerical Dynamics, 1000*, 1–20.
Johnson, G. R., & Morawska, L. (2009). The mechanism of breath aerosol formation. *Journal of Aerosol Medicine and Pulmonary Drug Delivery, 22*(3), 229–237.
Katz, J., & Sheng, J. (2010). Applications of holography in fluid mechanics and particle dynamics. *Annual Review of Fluid Mechanics, 42*, 531–555.
Kumar, S. S., Shao, S., Li, J., He, Z., & Hong, J. (2020). *Droplet evaporation residue indicating SARS-COV-2 survivability on surfaces*. arXiv preprint arXiv:2005.12262.
Lewis, D. (2020). Is the coronavirus airborne? Experts can't agree. *Nature, 580*(7802), 175–178.
Liu, Y., Ning, Z., Chen, Y., Guo, M., Liu, Y., Gali, N. K., … Liu, X. (2020). Aerodynamic analysis of SARS-CoV-2 in two Wuhan hospitals. *Nature, 582*(7813), 557–560.
Liu, T., & Shen, L. (2008). Fluid flow and optical flow. *Journal of Fluid Mechanics, 614*, 253–291.
Lu, J., Gu, J., Li, K., Xu, C., Su, W., Lai, Z., & Yang, Z. (2020). COVID-19 outbreak associated with air conditioning in restaurant, Guangzhou, China, 2020. *Emerging Infectious Diseases, 26*(7), 1628–1631.
Mangili, A., & Gendreau, M. A. (2005). Transmission of infectious diseases during commercial air travel. *The Lancet, 365*(9463), 989–996.
Memarzadeh, F., & Xu, W. (2012). March). Role of air changes per hour (ACH) in possible transmission of airborne infections. In *Building simulation* (Vol. 5, pp. 15–28). Tsinghua Press. No. 1.
Miserocchi, G., & Milic-Emili, J. (1976). Effect of mechanical factors on the relation between rate and depth of breathing in cats. *Journal of Applied Physiology, 41*(3), 277–284.
Morawska, L., Afshari, A., Bae, G. N., Buonanno, G., Chao, C. Y. H., Hänninen, O., & Salthammer, T. (2013). Indoor aerosols: From personal exposure to risk assessment. *Indoor Air, 23*(6), 462–487.
Morozov, V. N., & Mikheev, A. Y. (2017). A collection system for dry solid residues from exhaled breath for analysis via atomic force microscopy. *Journal of Breath Research, 11*(1), Article 016006.
Ong, S. W. X., Tan, Y. K., Chia, P. Y., Lee, T. H., Ng, O. T., Wong, M. S. Y., & Marimuthu, K. (2020). Air, surface environmental, and personal protective equipment contamination by severe acute respiratory syndrome coronavirus 2 (SARS-CoV-2) from a symptomatic patient. *Journal of the American Medical Association, 323*(16), 1610–1612.
Papineni, R. S., & Rosenthal, F. S. (1997). The size distribution of droplets in the exhaled breath of healthy human subjects. *Journal of Aerosol Medicine, 10*(2), 105–116.
Poon, T. C., & Liu, J. P. (2014). *Introduction to modern digital holography: With MATLAB*. Cambridge University Press.
Powers, M. C. (1953). A new roundness scale for sedimentary particles. *Journal of Sedimentary Research, 23*(2), 117–119.
Prather, K. A., Wang, C. C., & Schooley, R. T. (2020). Reducing transmission of SARS-CoV-2. *Science, 26*, 1422–1424.
Ranz, W. E., & Marshall, W. R. (1952). Evaporation from drops. *Chemical Engineering Progress, 48*(3), 141–146.
Stadnytskyi, V., Bax, C. E., Bax, A., & Anfinrud, P. (2020). The airborne lifetime of small speech droplets and their potential importance in SARS-CoV-2 transmission. *Proceedings of the National Academy of Sciences, 117*(22), 11875–11877.
Tang, J. W. (2009). The effect of environmental parameters on the survival of airborne infectious agents. *Journal of The Royal Society Interface, 6*, S737–S746.
Tobin, M. J., Chadha, T. S., Jenouri, G., Birch, S. J., Gazeroglu, H. B., & Sackner, M. A. (1983). Breathing patterns: 1. Normal subjects. *Chest, 84*(2), 202–205.
Van Doremalen, N., Bushmaker, T., Morris, D. H., Holbrook, M. G., Gamble, A., Williamson, B. N., … Lloyd-Smith, J. O. (2020). Aerosol and surface stability of SARS-CoV-2 as compared with SARS-CoV-1. *New England Journal of Medicine, 382*(16), 1564–1567.
Wan, M. P., Sze To, G. N., Chao, C. Y. H., Fang, L., & Melikov, A. (2009). Modeling the fate of expiratory aerosols and the associated infection risk in an aircraft cabin environment. *Aerosol Science and Technology, 43*(4), 322–343.
World Health Organization. (2004). Practical guidelines for infection control in health care facilities. available at: https://apps.who.int/iris/handle/10665/206946.
Yu, X., Hong, J., Liu, C., & Kim, M. K. (2014). Review of digital holographic microscopy for three-dimensional profiling and tracking. *Optical Engineering, 53*(11), 112306.
Zhai, Y., Li, X., Wang, T., Wang, B., Li, C., & Zeng, G. (2018). A review on airborne microorganisms in particulate matters: Composition, characteristics and influence factors. *Environment International, 113*, 74–90.
Zieger, P., Väisänen, O., Corbin, J. C., Partridge, D. G., Bastelberger, S., Mousavi-Fard, M., & Nenes, A. (2017). Revising the hygroscopicity of inorganic sea salt particles. *Nature Communications, 8*(1), 1–10.
Zou, L., Ruan, F., Huang, M., Liang, L., Huang, H., Hong, Z., & Guo, Q. (2020). SARS-CoV-2 viral load in upper respiratory specimens of infected patients. *New England Journal of Medicine, 382*(12), 1177–1179.